

Functional Analysis of Mitral Complex Geometry using Support Vector Machines from 3D Echocardiography

Wei Song¹, Xin Yang¹, Jing Wang², Yi Yu³, Sun Kun³

¹Institution of Image Processing and Pattern Recognition, Shanghai Jiao Tong University, Shanghai, China

²Shanghai Children's Medical Center, Medical College, Shanghai Jiao Tong University, Shanghai, China

³Xinhua Hospital, School of Medicine, Shanghai Jiao Tong University, Shanghai, China

Abstract

In order to assist diagnosis and surgical repair of congenital mitral disease, quantitative analysis of 3D geometry of the mitral complex is necessary for better understanding mechanism and dysfunction of the mitral complex. This work aims to extract geometric parameters of mitral complex and utilize Support Vector Machines (SVM) based classifier to support diagnosis of congenital mitral regurgitation (MR). With a control group of 20 normal young children (11 boys, 9 girls, 5.96 ± 3.12 years) with normal structure of mitral apparatus, 20 patients (9 boys, 11 girls, 5.59 ± 3.30 years) suffering from severe congenital MR are recruited in this study. The results of parameter validation demonstrates that the measurement precision is in the range of inter-/intra-observer variability. SVM-based classifier achieves average classification accuracy at 85.0% in the present population.

1. Introduction

Quantitative analysis of 3D geometry of mitral apparatus during the cardiac cycle is necessary for understanding the 'pump' role of the mitral valves and mechanism of its malfunction, assessment of mitral function, pathology diagnosis and surgical planning. Many literatures on mitral regurgitation (MR) have been published on adult ischemic mechanism of MR [1], but the mechanism of MR caused by congenital mitral dysfunction is still open.

From an anatomic point of view, mitral apparatus can be regarded as a functional complex comprising mitral annulus (MA), mitral leaflets, chorda tendineae, and papillary muscles, and their geometric features characterize the behavior of mitral valves. Mitral tension

device that is in control of mitral leaflets' motion consists of chorda tendineae and papillary muscles [2-5]. Accordingly, it is necessary to have a relative comprehensive evaluation of the mitral apparatus [6].

Several previous researches have dealt with geometry of mitral complex. 2D projected area and 3D surface area of MA are estimated during systole in [7]. Reference values describing the shape and size of MA and the position of papillary muscles in normal individuals are measured in 2D views under the assumption of elliptic geometry [6]. Three parameters regarding assumed two peaks and two troughs of saddle-shaped annulus are presented to assess the non-planar shape of the MA [8].

In this work, from a simple configuration of the mitral complex, five measurements that quantitatively characterize its geometry and function in a new 3D local coordinate system are calculated. These measurements are about the size of MA and the position of the papillary muscles to get insights into the function and malfunction of mitral apparatus. Then Support Vector Machines (SVM) classifier recognizes patients suffering from severe congenital MR and normal young children with normalized geometric parameters. Our method provides a possibility to explore the relationship between geometry of mitral apparatus and congenital mitral disease and would be a guide for proper strategy in surgical repair.

2. Method

2.1. 3D reconstruction of mitral complex

In the cross-sectional planes along the long axis direction of left ventricle, two hinge points, the junction points between the annulus and the leaflets, are selected as feature points on the annulus. Because these hinge points are sampled in arbitrary order in 3D space, the rearrangement must be done. Then a closed annular curve is fitted with the non-uniform rational B-Spline (NURBS)

algorithm, and modified to make it pass through all the hinge points.

The proposed reconstruction of MA defines the shape of the mitral valves regardless of the free margin of leaflets. More valuable or accurate analytical outcomes about function of mitral apparatus would be obtained, especially involving chordae tendineae and papillary muscles, which play the role of traction force on the valve leaflets [2, 4, 5]. Then antero-lateral and postero-medial papillary muscle tips act on chordae tendineae are taken into account. Finally, a simple configuration approximately describes anatomical geometry of the mitral complex.

In order to avoid influence of inherent motion of scanning probe, body and heart, a reference plane is defined as the least-squares plane that is fitted to the annular curve minimizing the expression

$$g(A, B, C) = \frac{\sum (z_i - Ax_i - By_i - C)^2}{A^2 + B^2 + 1}$$

where A , B , C are the coefficients of the plane $f(x, y, z) = z - Ax - By - C = 0$. Accordingly, a new local Cartesian coordinate system is established to make compensation, where the XOY plane is identical to the reference plane and the Z axis is parallel to the normal vector of the reference plane.

2.2. Estimation of geometry of mitral complex

Geometric parameters of the mitral apparatus proposed in the previous researches can be derived and compared convincingly in the above coordinates of the mitral apparatus.

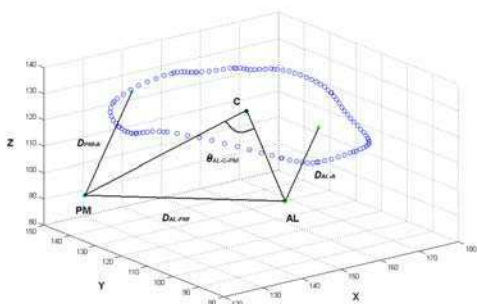


Figure 1. Definition of anatomical feature points and geometric measurements of the mitral apparatus. AL, antero-lateral papillary muscle tip; PM, postero-medial papillary muscle tip; C, annular center; D_{AL-A} , AL papillary annular distance; D_{PM-A} , PM papillary annular distance; D_{AL-PM} , inter-papillary distance between papillary muscle tips; $\theta_{AL-C-PM}$, papillary muscle angle measured between the two lines connecting annulus center and papillary muscle tips.

In our work, five geometric measurements are adopted as showed in Figure 1. Annular area is a classical descriptor of geometry and function of mitral valves [9]. Different from the area of 3D surface [7] and the area in 2D echocardiography [6], the effective area of the annulus is regarded as the area of 3D surface of the mitral valves projected onto the best fitting annular reference plane, denoted by S_A . Papillary muscle angle measured between the two lines connecting annulus center and papillary muscle tips is denoted by $\theta_{AL-C-PM}$. Meantime inter-papillary distance measured between both papillary muscle tips (D_{AL-PM}) and papillary annular distances (D_{AL-A} , D_{PM-A}) are obtained in the 3D space, also different from the pre-proposed measurements in [5] regarding the papillary muscles and the MA in 2D echocardiography. D_{AL-A} is the distance from the antero-lateral papillary muscle tip to the best fitting annular reference plane, and D_{PM-A} is for the postero-medial papillary muscle tip. These four parameters present the 3D spatial relationship between apparatus beneath the valves and MA.

All these geometric parameters are calculated at end-systole and end-diastole, determined in our work as follows; end-systole: the frame corresponding to the peak of T-wave, end-diastole: the frame corresponding to the peak of QRS-wave in the electrocardiogram.

Especially for children, individual variability of cardiac growth is obviously great. Therefore, in order to compare the geometric parameters of the mitral apparatus between normal young children and patients, they might be normalized by a certain reference value as a compensation for difference of age, gender and body habitus, such as BSA or LV end-diastolic Volume [10]. In our work, BSA calculated on BSA Calculator developed by ChemDrug, Co. [11] is chosen as the normalization reference value.

2.3. Statistical analysis

The data are expressed as mean \pm SD. For each parameter, inter-observer and intra-observer reliability are calculated using Bland-Altman method. It determines the agreement between measurements by calculating the bias (mean difference) and limits of agreement (1.96 standard deviations of the difference) [12].

To distinguish patients with congenital MR from the normal children from our acquired multiple geometric parameters of mitral apparatus, it can be served by multidimensional classification method. As a representative of nonlinear classification method, SVM is taken in our case to classify the acquired data. More details regarding SVM can be found in [13].

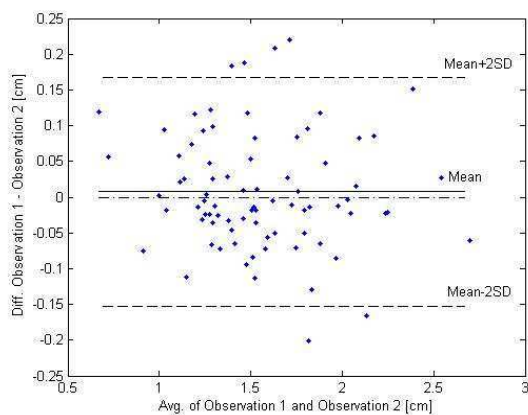
3. Experiments and results

3.1. Data and population

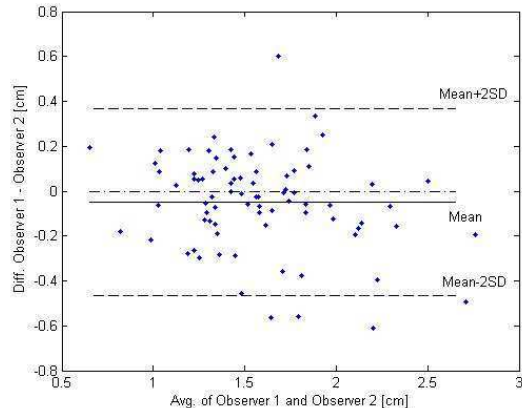
RT3DE scanning is performed with a commercial available system (Sonos 7500, Philips, Co.) in Shanghai Children’s Medical Center of Shanghai Jiao Tong University. The 3D echocardiographic images are recorded at 15.9 ± 3.1 (range 9-24) frames per cardiac cycle and formatted into a $208 \times 160 \times 144$ data set.

20 normal young children (Group ω_n , 11 boys, 9 girls, 5.96 ± 3.12 years) are selected, compared with 20 patients (Group ω_{mr} , 9 boys, 11 girls, 5.59 ± 3.30 years) with moderate-to-severe MR due to congenital malfunction or secondary disease of the mitral valves. Color transthoracic Doppler echocardiography is employed to assess the severity of MR by the regurgitation jet.

3.2. Reliability of measurements and quantitative analysis



(a)



(b)

Figure 2. Bland-Altman plots for geometric parameter D_{AL-A} between two measurements by the same observer (a) and by two different observers (b).

To assess the reproducibility of mitral apparatus quantification, the measurements are repeated two weeks later by the same observer who is blinded to the results of

any previous measurements, and inter-observer reliability is calculated on measurements conducted by two doctors independently. Bland-Altman plots are given in Figure 2(a) and (b). For each parameter, mean bias and confidence range (CR) ($\text{mean} \pm 1.96\text{std}$) are summarized in Table 1, and p presents the percentage of points outside the limits of agreement. The results indicates that there is a small but significant underestimation ($p < 0.05$) with a bias of 0.001 in intra-observer measurement for S_A , and both intra-observer and inter-observer measurements for other parameters has good agreement.

Table 1. Mean difference and confidence range of intra-observer and inter-observer measurements for each geometric parameter.

Parameter	Inter-observer			Intra-observer		
	Mean	CR	p	Mean	CR	p
$S_A(\text{cm}^2)$	0.042	[-0.308,0.392]	0.075	0.001	[-0.510,0.512]	0.038
$D_{AL-A}(\text{cm})$	0.008	[-0.153,0.168]	0.075	-0.049	[-0.463,0.366]	0.063
$D_{PM-A}(\text{cm})$	0.005	[-0.208,0.219]	0.063	0.036	[-0.413,0.486]	0.050
$D_{AL-PM}(\text{cm})$	0.009	[-0.195,0.212]	0.063	-0.026	[-0.441,0.389]	0.050
$\theta_{AL-C-PM}(\circ)$	0.136	[-6.153,6.425]	0.063	0.415	[-10.311,11.140]	0.075

Table 2. Comparison of BSA-normalized geometric parameters of the mitral apparatus between group ω_n and ω_{mr} at end-diastole and end-systole.

Parameter	At end-systole		At end-diastole	
	Group ω_n	Group ω_{mr}	Group ω_n	Group ω_{mr}
$S_A(\text{cm}^2)$	4.53 ± 0.79	10.43 ± 3.59	5.29 ± 0.96	11.96 ± 4.10
$D_{AL-A}(\text{cm})$	1.76 ± 0.36	1.83 ± 0.57	1.96 ± 0.32	2.44 ± 0.58
$D_{PM-A}(\text{cm})$	1.99 ± 0.36	2.30 ± 0.58	2.39 ± 0.48	3.11 ± 0.95
$D_{AL-PM}(\text{cm})$	1.67 ± 0.44	2.60 ± 0.81	2.42 ± 0.51	3.69 ± 1.32
$\theta_{AL-C-PM}(\circ)$	58.10 ± 22.46	75.22 ± 32.32	69.81 ± 23.60	85.78 ± 43.12

Table 2 summarizes geometric parameters normalized by BSA to compensate for individual difference of age and gender. Effective annular area S_A in children with severe MR is considerable larger than in normal subjects both at end-systole and end-diastole. Papillary muscle angle is secondary remarkable different between the normal and patients. That Papillary annular distance D_{AL-A} is relatively less differentiable between two groups may reveal the position of antero-lateral papillary muscle tip is stable relative to the annular fitting plane. Papillary annular distance D_{PM-A} changes more than D_{AL-A} from end-systole to end-diastole, it shows the motion range of postero-medial papillary muscle is less than that of antero-lateral papillary muscle [5]. And then inter-papillary distance D_{AL-PM} in the normal group is smaller than that in the patient group.

3.3. Classification problem

In our work, degree 2 Polynomial SVM with some tolerance to misclassification errors (regularization parameter $C=5$) is employed, especially for the present

size of data.

Due to the limited amount of training data, mean error rate with 'Leave-One-Out' method [14] is calculated as the estimation of classification error rate for unknown test data. For each parameter in two-phase as input, the classification results are in Table 3. Then all geometric parameters (in a single column vector form) are fed into SVM classifier with results showed in Table 4.

The performance of SVM classifier is evaluated in terms of sensitivity, and specificity given by

$$Se = \frac{T_p}{P} \times 100\%; Sp = \frac{T_N}{N} \times 100\%$$

where Se and Sp are sensitivity and specificity, respectively. T_p is the number of true positive predicted, T_N is the number of true negative predicted, P is the number of actual positives, and N is the number of actual negatives. In our case, MR children are labeled negatives and controls are positives.

Table 3. Error rate, specificity and sensitivity of SVM classification for each normalized parameter.

Parameters	Err(%)	Sens(%)	Spec(%)
S_A	10.00	90.00	90.00
D_{AL-A}	17.50	90.00	75.00
D_{PM-A}	37.50	65.00	60.00
D_{AL-PM}	17.50	95.00	70.00
$\theta_{AL-C-PM}$	22.50	70.00	85.00

Table 4. Error rate, specificity and sensitivity of SVM classification for all normalized geometric parameters.

Err(%)	Sens(%)	Spec(%)
15.00	85.00	85.00

The results in Table 3 suggest that descending sort with respect to separability of each geometric parameter is S_A , D_{AL-A} , D_{AL-PM} , $\theta_{AL-C-PM}$ and D_{PM-A} . And the results in Table 4 indicate that fed with all geometric parameters in a single column form, SVM classifier performs excellent with 15% error rate.

4. Conclusions

The results of parameter validation and SVM classification in the present population indicates that this work provides a practical tool for quantitative analysis of 3D geometry of mitral apparatus that could support diagnosis and surgical treatment of its dysfunction.

Acknowledgements

This paper has been partially supported by National Basic Research Program of China (2010CB732506) and Shanghai Basic Research Program (09jc1410502).

References

- [1] Watanabe N, Ogasawara Y, Yamaura Y, Wada N, Kawamoto T, Toyota E, Akasaka T, Yoshida K. Mitral annulus flattens in ischemic mitral regurgitation: geometric differences between inferior and anterior myocardial infarction. *Circulation* 2005; 112: 458-462.
- [2] Allen HD, Driscoll DJ, Shaddy RE, Feltes TF. *Moss and Adams' Heart Disease in Infants, Children, and Adolescents*, 7th Edition. Lippincott Williams & Wilkins, Philadelphia, 2007: 2-47.
- [3] Gorman JH, Jackson BM, Enomoto Y. The effect of regional ischemia on mitral annular saddle shape. *Annals of Thoracic Surgery* 2004; 77: 544-548.
- [4] Timek TA, Lai DT, Tibayan F. Annular versus subvalvular approaches to acute ischemic mitral regurgitation. *Circulation* 2002; 106:127-132.
- [5] He S, Jimenez J, He Z. Mitral leaflet geometry perturbations with papillary muscle displacement and annular dilatation: an in-vitro study of ischemic mitral regurgitation. *The Journal of Heart Valve Disease* 2003; 12: 300-307.
- [6] Nordblom P, Bech-Hanssen O. Reference values describing the normal mitral valve and the position of the papillary muscles. *Echocardiography* 2007; 24:665-672.
- [7] Kwan J, Jeon M, Kim D, Park K, Lee W. Does the mitral annulus shrink or enlarge during systole? A real-time 3D echocardiography study. *Journal of Korean Medical Science* 2009; 24: 203-208.
- [8] Zhu L, Yang X, Yao L, Sun K. Three dimensional reconstruction and dynamic analysis of mitral annular based on connected equi-length curve angle chain. *Lecture Notes in Computer Science* 2007; 4901: 298-306.
- [9] Frangi AF, Niessen WJ, Viergever MA. Three-dimensional modeling for functional analysis of cardiac images: A Review. *IEEE Transaction on Medical Imaging* 2001; 20: 2-25.
- [10] Kaski JP, Daubney PEF. Normalization of echocardiographically derived paediatric cardiac dimensions to body surface area: time for a standardized approach. *European Journal of Echocardiography* 2009; 10: 44-4.
- [11] <http://www.chemdrug.com>
- [12] Bland JM, Altman DG. Statistical methods for assessing agreement between two methods of clinical measurement. *Lancet* 1986; 327: 307-310.
- [13] Burges CJC. A tutorial on support vector machines for pattern recognition. *Data Mining and Knowledge Discovery* 1998; 2: 121-167.
- [14] Duda RO, Hart PE, Stork DG. *Pattern Classification*, 2nd Edition. John Wiley & Sons, Inc., New York, 2001.

Address for correspondence.

Wei Song

Room 220, No.2 SEIEE Building, Shanghai Jiao Tong University, No.800, Dong Chuan Road, Shanghai 200240, China.

esong1029@hotmail.com